



UPPSALA
UNIVERSITET

UPTEC K13016

Examensarbete 30 hp
Augusti 2013

Optical and Mechanical Properties of Cool Roof Paint Containing Hollow Thermoplastic Microspheres

Olof Sandin



UPPSALA
UNIVERSITET

**Teknisk- naturvetenskaplig fakultet
UTH-enheten**

Besöksadress:
Ångströmlaboratoriet
Lägerhyddsvägen 1
Hus 4, Plan 0

Postadress:
Box 536
751 21 Uppsala

Telefon:
018 – 471 30 03

Telefax:
018 – 471 30 00

Hemsida:
<http://www.teknat.uu.se/student>

Abstract

Optical and Mechanical Properties of Cool Roof Paint Containing Hollow Thermoplastic Microspheres

Olof Sandin

This master thesis examines the effect of hollow thermoplastic microspheres in cool roof paints. These types of paints are characterized by their high reflectivity for wavelengths up to 2.5 micrometers and high absorptivity in the IR region. The thermoplastic microspheres were produced by Expancel®, a unit within AkzoNobel®. Optical properties were measured using a UV-VIS-NIR spectrophotometer and FTIR. The paint systems were kept as simple as possible, only containing binder, pigment and additive, thus limiting the study to relative comparisons. TiO₂ was used as standard pigment. The additive component was varied between thermoplastic, glass or ceramic microspheres. The reference sample used CaCO₃ as additive. The microsphere particle size was found to have the greatest impact on the paints reflectivity. The smallest microsphere tested in this study, with a diameter of around 10 micrometers was also the best performing. Absorptance and emittance were not found to be affected by incorporating microspheres into the paint. Thermoplastic microspheres that were coated with TiO₂, called coexpanded microspheres were also tested. The incorporation of coexpanded microspheres showed no increase in reflectivity compared to other paints containing thermoplastic microspheres. Four different paint systems were color matched (blue) at a local paint shop in order to examine non-white paints as well. Paints containing thermoplastic microspheres performed better than paints using any of the other additives, regardless if the paints were white or non-white.

Handledare: Jan Nordin
Ämnesgranskare: Annica Nilsson
Examinator: Karin Larsson
ISSN: 1650-8297, UPTec K13016

Sammanfattning

I detta examensarbete undersöktes effekten av ihåliga termoplastiska mikrosfärer i "cool roof paints". Dessa typer av färger kännetecknas av hög reflektivitet upp till 2,5 μm och hög absorptionsförmåga för längre våglängder. De termoplastiska mikrosfärerna producerades av Expancel®, en del av AkzoNobel®. Optiska egenskaper mättes med UV-VIS-NIR spektrofotometer och FTIR. Färgerna hölls så enkla som möjligt, endast innehållandes bindemedel, pigment och additiv. På så sätt begränsades studien till relativa jämförelser. TiO_2 användes som standardpigment. Additiven varierades mellan termoplastiska, glas eller keramiska mikrosfärer. Referensprovet använde CaCO_3 som additiv. Mikrosfärernas storlek hade störst påverkan på färgernas reflektivitet. Den minsta mikrosfär som testades i denna studie hade en diameter på cirka 10 μm och var också den bäst presterande med avseende på optiska egenskaper. Absorption och emittans tycktes ej påverkas av förekomsten av mikrosfärer. Termoplastiska mikrosfärer belagda med TiO_2 , så kallade samexpanderade mikrosfärer, undersöktes också. Resultaten visade ingen skillnad mellan samexpanderade och "vanliga" mikrosfärer. Fyra opigmenterade färger lämnades in till en lokal färghandel för att brytas i samma blåa färg. Färger som innehöll termoplastiska mikrosfärer presterade bättre i de optiska mätningarna än de färger som innehöll något av de andra additiven.

Table of Contents

1	Introduction.....	1
1.1	Background.....	1
1.2	Aim.....	2
2	Theory	3
2.1	Cool Roof Paint.....	3
2.2	Expancel® Microspheres	8
2.3	Paint.....	10
2.4	Spectrophotometry	11
2.5	Fourier Transform Infrared Spectroscopy (FTIR)	11
3	Experimental.....	13
3.1	Paint formulations	13
3.2	Dirt Pick-Up	15
3.3	Optical Measurements	15
3.4	Contact Angle.....	15
4	Results and Discussion	16
4.1	Optical Measurements	16
4.2	Coexpanded Spheres	23
4.3	Dirt Pick-Up.....	25
4.4	Contact Angle.....	26
4.5	Filler (CaCO ₃).....	27
5	Conclusions and Future Work	28
	Acknowledgments	28
	References.....	29
	Appendix A.....	31
	Appendix B.....	32

1 Introduction

1.1 Background

The urban heat island effect increases the temperature in urban areas. It is a well known and well studied phenomenon [1-4]. The major causes of urban heat islands are street canyon geometry and heat absorption by buildings [2]. This is mainly a problem in warmer climates. Akbari et al. reports that the temperature in urban areas can be around 2.5 °C higher than surrounding areas in the summer [4]. They also state that for every 1 °C increase in temperature, peak electricity demand rises by 2 – 4%. According to the US Energy Information Administration, buildings stand for 72% of the electric energy use in the US and 14% of this stems from cooling [5]. This means that the energy usage of AC units has a substantial impact on energy consumption. By increasing the overall albedo of urban areas, the radiative energy that is absorbed by low albedo surfaces can instead be reflected back into the atmosphere. Lower roof surface temperature means less heat transferred to the indoor environment and decreased cooling demands. Higher albedo roofs could decrease the peak energy demand during hot summer months and increase the indoor comfort of buildings without AC units. Taha has modeled how high albedo surfaces in urban environments can help mitigate the urban heat island effect. He also found that it could reduce ground level ozone (precursor to smog) which is a serious problem in some of the worlds larger cities [6,7]. The key behind increasing the albedo of buildings lies in the optical properties of the surface. By painting the roof with a highly reflective and thermally emitting paint (so called cool roof paint), less energy is absorbed and transferred into the building. Previous unpublished studies performed at Expancel®, a unit within AkzoNobel® where this master thesis is conducted, have indicated that the addition of thermoplastic microspheres to roof paint increases the total solar reflectance (TSR, also known as R_{sol}). More studies are needed to help understand the reason behind this increase and to be able to optimize the system.

The awareness of urban heat island mitigation through the use of cool roofs has grown substantially in the last decade, especially in the U.S. Examples are the California Energy Commission's title-24 Building Efficiency Standards which set up concrete requirements for roof products [8]. The standards are based on the recommendations from the Cool Roof Rating Council, which is a non-profit organization. The City of Chicago requires that all low slope roofs are built in accordance with the U.S. Environmental Protection Agency's Energy Star cool roof standards [9]. Both Philadelphia and New York City have taken initiatives to implement cool roofs in new constructions [10].

1.2 Aim

The aim of this master thesis is to examine the effect of thermoplastic microspheres in reflective roof coatings known as cool roof paints, increase knowledge of the optical properties of the microspheres and examine the interaction between microspheres and the white pigment TiO_2 . Previous studies have shown that the R_{sol} of paints increases with decreasing diameter of the microspheres. It is also a known fact that TiO_2 is an excellent reflective pigment in the visual part of the electromagnetic spectrum and is used by paint manufacturers as a white pigment. This pigment is relatively expensive so if the addition of microspheres to a reflective paint increases the R_{sol} , two possibilities arise. The first is being able to produce a superior cool roof paint, the second is being able to technically match other commercial alternatives but with less TiO_2 .

The plan was to prepare different paint formulations with different volume fractions of microspheres, while keeping the amount of TiO_2 constant. To be able to continue the evaluation of the correlation between R_{sol} and particle size, both 10 μm and 20 μm spheres were studied. A recently developed expansion technique where the microspheres are coated with TiO_2 -particles instead of just being separately mixed into the paint was also included in the project. Alternative commercial additives such as glass and ceramic spheres were included to be able to examine any differences compared to the thermoplastic spheres. Optical properties such as reflectance and emittance are determined at Uppsala University using a spectrophotometer and an FTIR instrument. Contact angle measurements and dirt pick-up studies were conducted at SP Technical Research Institute of Sweden in Stockholm.

2 Theory

2.1 Cool Roof Paint

The performance of cool roof paints is mainly governed by their optical properties. The sun emits electromagnetic radiation which hit the earth's atmosphere. The resulting spectrum after atmospheric absorption is illustrated in fig. 1.

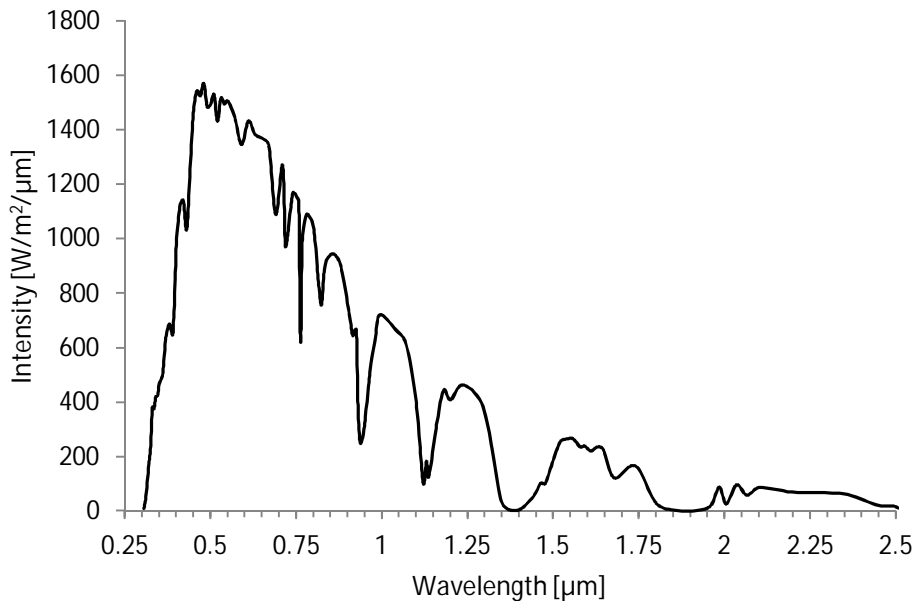


Figure 1. Solar spectrum at sea level (air mass 1.5) according to ISO 9845.

The intensity of the solar radiation peaks in the visual part of the spectrum but that part of the solar spectrum only contains about 45% of the energy. The peak which is located around 555 nm coincides with the maximum relative sensitivity of the human eye in daylight conditions, see fig. 2d. The solar spectrum can be divided into UV < 380 nm, VIS 380 – 780 nm and NIR 780 – 2500 nm. The intensity in the UV part of the spectrum at sea level is rather low due to atmospheric absorption which means that the NIR part of the spectrum contains a substantial amount of the incoming radiative energy, around 50%. This “invisible” part of the spectrum plays a major role in cool roof paints. As previously mentioned, by reflecting incoming radiation from the sun, less energy (heat) is absorbed by the surface. A paint's emittance determines its ability to radiate heat to its surroundings via IR (for relatively low temperatures) radiation, thus cooling itself. The reflectivity and emissivity of a material are closely related via eq. 1 and 2. The earth cools itself via the atmospheric window, positioned between 8 – 13 μm in the IR portion of the spectrum, where the atmospheric absorption is at a minimum, see fig. 2c.

A material with high emissivity is thus able to emit thermal radiation (IR) back into the atmosphere, or space if the wavelength matches the atmospheric window, and subsequently cooling the surface. Fig. 2 illustrates the boundary conditions of cool roof paints.

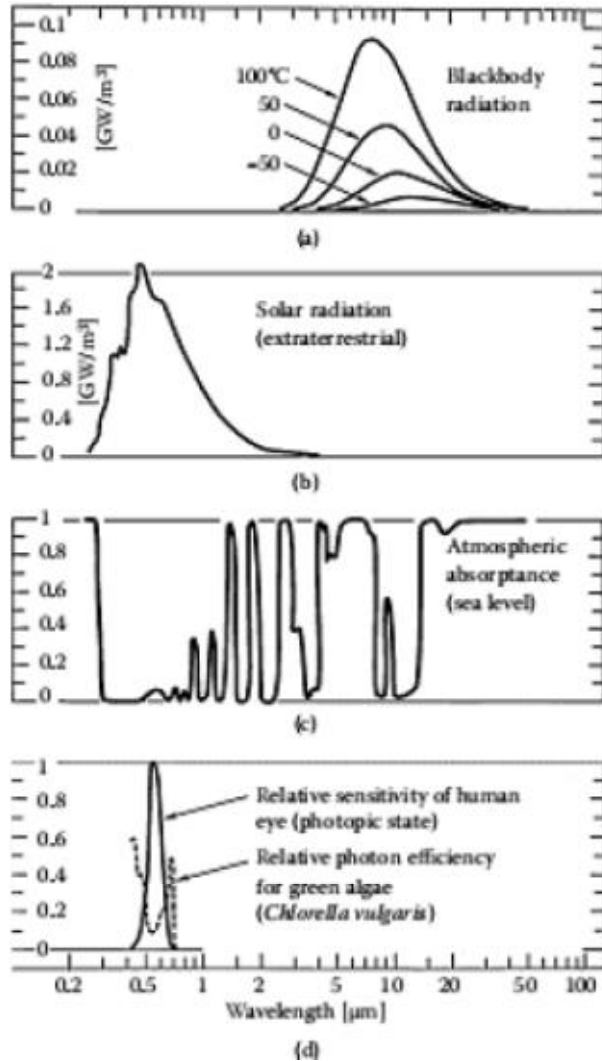


Figure 2. (a) Blackbody radiation at different temperatures. Increasing the temperature pushes the maximum towards shorter wavelengths. (b) The spectrum of the solar radiation before it passes through the earth's atmosphere. (c) The atmospheric absorptance spectrum. The atmospheric window is located between 8 – 13 μm and is characterized by its low absorption. (d) The relative sensitivity of the human eye whose maximum coincides with the solar radiation peak [11].

The extraterrestrial solar radiation is similar to a 6000 K blackbody radiator. The atmospheric absorption is responsible for the difference between fig. 1 and 2b. Figure 2a illustrates how the radiation peak for blackbody radiators is dependent on temperature; higher temperature pushes the peak towards lower wavelengths. The large difference in temperature between the sun and for example a roof surface explains why they emit radiation at different wavelengths. The solar spectrum at sea

level spans from around 300 – 2500 nm while a roof surface emits radiation at longer wavelengths (see fig. 2a for blackbody radiators at 0 – 100 °C). There is a small overlap in the NIR area but the overall difference in wavelength for the two radiation sources is of great importance for an ideal cool paint. The basic principle when radiation strikes a material is that the radiation is reflected (R), transmitted (T) or absorbed (A) according to

$$A(\lambda) + R(\lambda) + T(\lambda) = 1 \quad (1)$$

Kirchoff's law states that for an object in thermal equilibrium, absorption at a certain wavelength λ is equal to the emittance (ε) at the same wavelength

$$A(\lambda) = \varepsilon(\lambda) \quad (2)$$

The ideal cool paint would reflect 100% of the solar spectrum, minimizing the amount of energy absorbed by radiation. The spectral selectivity becomes apparent in fig. 3 at 2500 nm where the sudden drop in reflectance from 100 to 0% takes place. For the wavelengths larger than 2500 nm, an ideal cool paint would act as a perfect blackbody and according to Kirchoff's law absorb, and consequently emit, 100% of the thermal radiation possibly resulting in subambient temperatures. An important factor in the paint industry is coverage. Good coverage means an opaque paint which eliminates the transmittance term from eq. 1 and simplifies it into

$$A(\lambda) + R(\lambda) = 1 \quad (3)$$

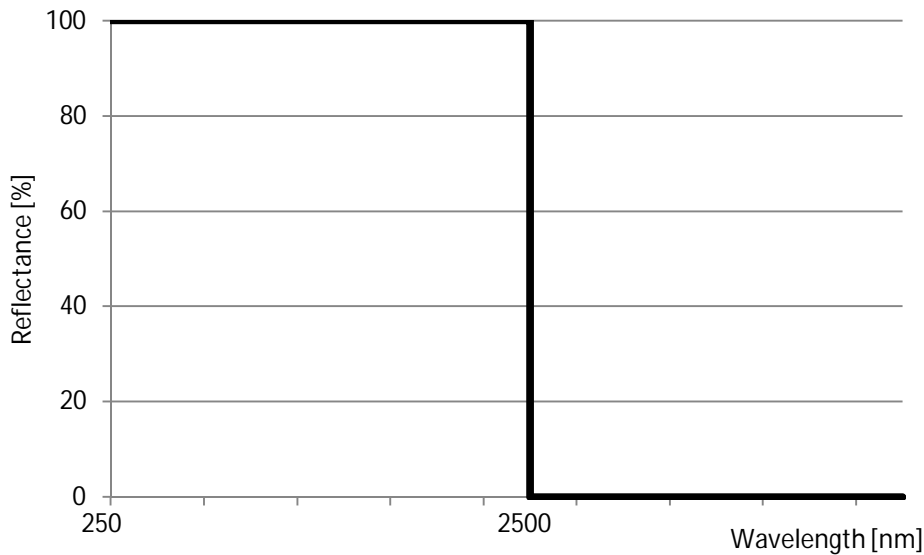


Figure 3. Reflectance spectrum of an ideal cool paint. In order to maximize both its reflectivity and emissivity at the right wavelengths, there is a sudden drop in reflectance at 2500 nm. All in accordance with equation 2 and 3.

The net effect of installing a cool roof depends on a number of parameters such as: insulation, type of roof, cooling needs, type of AC unit, geographic location etc. The effect of insulation has been studied by Simpson and McPhearson [12]. They concluded that the effect of installing a cool roof was larger for a poorly insulated house. If the building is located in a relatively cold climate, extra heating needs may occur during the winter. The net effect is in most cases positive due to the lower solar altitude of the sun in the winter plus the fact that the amount of sunshine in the summer exceeds the amount of sunshine in the winter. Levinson and Akbari published a paper in 2009 where they ran simulations on the effect of replacing standard roof paints with cool roof paints in the US [13]. They compared energy saving versus heating penalty in the winter and showed that the energy savings ranged from 3.30 kWh/m² in Alaska to 7.69kWh/m² in Arizona with a national average of 5.02 kWh/m² annually. The heating penalty ranged from 0.088 kWh/m² in Hawaii to 4.10 kWh/m² in Wyoming with a national average of 1.90 kWh/m². Levinson and Akbari used a reflectance value of 0.55 to represent a weathered white cool roof and 0.20 for the standard gray roof.

Solar reflectance index (SRI) is a measure on how “cool” a material is. SRI is based on the total solar reflectance and thermal emittance of the material and compares the materials steady state temperature to a black (T_{Black} , $R = 0.05$, $E = 0.90$, $SRI = 0$) and a white (T_{White} , $R = 0.80$, $E = 0.90$, $SRI = 100$) reference material.

$$SRI = \frac{T_{Black} - T_{Surface}}{T_{Black} - T_{White}} \cdot 100 \quad (4)$$

A surface which is hotter than the black reference material has a negative SRI value and a surface which is cooler than the white material has an SRI value > 100 [14]. Santamouris et al. lists a number of cool roof materials where the highest scoring materials in regard to SRI are white materials [15]. This is consistent with the fact that white materials are the most reflective materials in the visual part of the spectrum. In order to calculate a material's SRI, both thermal emittance and its R_{sol} has to be calculated. R_{sol} is calculated by weighting the materials reflectance with the solar radiation (see fig. 1) in accordance with equation 5.

$$R_{sol} = \frac{\int_{\lambda_1}^{\lambda_2} R(\lambda) \Phi(\lambda) d\lambda}{\int_{\lambda_1}^{\lambda_2} \Phi(\lambda) d\lambda}, \quad (5)$$

where $R(\lambda)$ is the material's reflectance and $\Phi(\lambda)$ the solar radiation [16]. The thermal emittance is calculated in a similar fashion as R_{sol} but instead of using the solar radiation as a weighting factor, blackbody radiation at a given temperature (in this study, 323 K) is used. Blackbody radiation is calculated in accordance with equation 6.

$$G = \frac{2\pi hc^2}{\lambda^5 e^{\frac{hc}{\lambda kT}} - 1}, \quad (6)$$

where h is the Planck constant, c is the speed of light in vacuum, λ is the wavelength, k is the Boltzmann constant and T is the absolute temperature. The SRI is applicable to low slope roofs. Roofs with steeper slopes, more common on residential buildings, may produce glare if they are white. By switching to another color, you will always reduce the reflectance in the visual part of the spectrum. The answer to this problem is finding a pigment or additive that enhances the reflectivity in the NIR part of the spectrum. Synnefa et al. published a paper where they used special IR reflecting pigments to enhance the R_{sol} . They managed this without changing the visual appearance of the paint, i.e. using color matched paints [3].

Glare can also be a problem with a very smooth surface. Granqvist and Smith discusses the problem and states that a smooth black surface can produce more glare than a not so smooth white surface [17]. The reflectance is affected by the smoothness of the surface. A rough surface increases the probability of absorption due to the fact that the incoming photon may have to reflect multiple times before being able to leave the surface [18]. Although the roughness of the surface has an impact on glare, the major contributor to glare is type of reflectance, specular or diffuse.

2.2 Expancel® Microspheres

The thermoplastic microspheres used in this study are produced at Expancel®, a part of AkzoNobel®, located at Stockviksverken south of Sundsvall. The microspheres are micrometer sized plastic hollow spheres. The production is based on a suspension polymerization where the organic phase mainly consists of monomers and blowing agent. The water phase contains an inorganic stabilizer and initiator, usually some sort of organic peroxide. By mixing the two phases with high speed stirring, tiny droplets of monomer and blowing agent is formed. The stabilizers keep the tiny droplets from coalescing by encapsulating them. Because the polymer is not soluble in the organic phase, it moves towards the phase boundary, i.e. the water/organic interface, and creates the shell of the microsphere. The hydrocarbon blowing agent is in that way still trapped inside the microsphere. Depending on the kind of monomers and blowing agents used, different amounts of heat are required to expand the now formed microspheres. When heat is added, the polymer reaches its glass transition temperature, T_g , and softens. In a well functioning process, the T_g should be carefully matched with the boiling point and/or expansion of the blowing agent. The expansion of the thermoplastic microspheres generates a large decrease in density, often in terms of $\sim 1100 \text{ kg/m}^3 \rightarrow \sim 30 \text{ kg/m}^3$. The shell hardens when the temperature drops below the T_g of the polymer shell. Fig. 4 is a thermomechanical analysis (TMA) diagram which illustrates the expansion progress in regard to increasing temperature ($20 \text{ }^\circ\text{C/min}$). The expansion starts at T_{start} and proceeds to T_{max} (around $105 \text{ }^\circ\text{C}$ and $145 \text{ }^\circ\text{C}$ respectively for this specific quality of microspheres) which coincides with the peak of the curve. The lowest density (greatest height at y axis) is achieved at T_{max} . Further increase in temperature causes the microspheres to collapse which leads to an increase in density. In this thesis, the expanded microspheres are added to the paint. In other applications, the unexpanded microspheres are used as the finished product. All depending on which properties are sought.

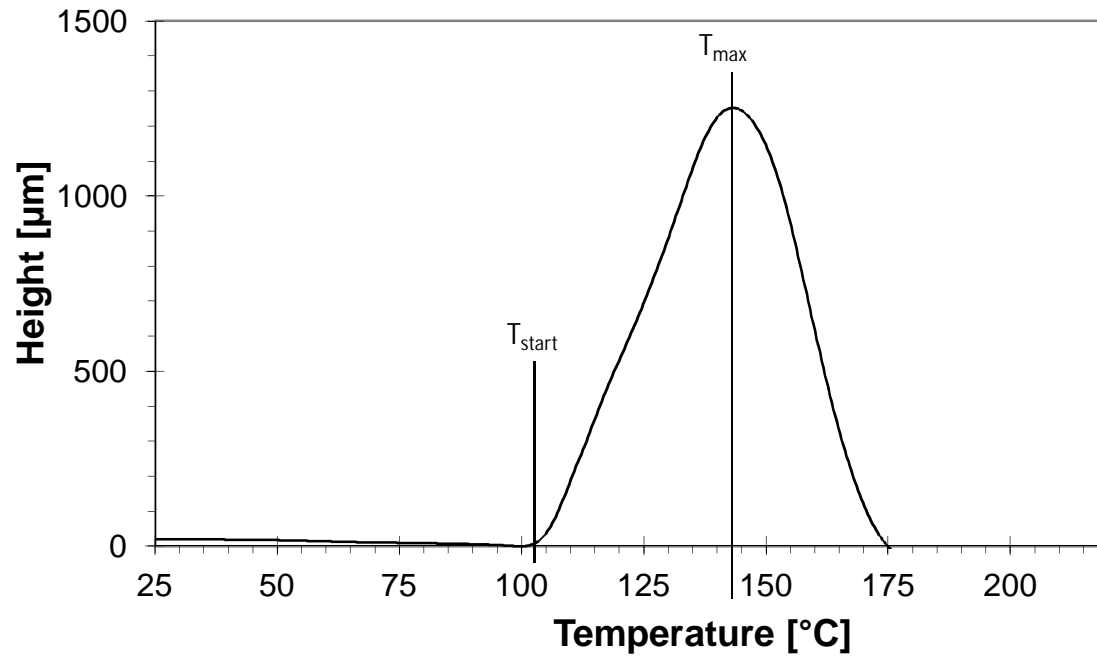


Figure 4. Thermomechanical analysis (TMA) diagram illustrating the temperature dependency of the expansion process. The lowest microsphere density is achieved at the top of the curve, at approximately 145 °C. The height that is depicted at the y-axis is a measurement of the displacement of the probe which is an effect of the expansion that is taking place as the temperature exceeds T_{start} .

The hollow microspheres exert foam like behavior regarding their reflective properties, both being a multiple scattering medium. Liquid foam consists of thin walled bubbles which encapsulate air, very similar to the thermoplastic microspheres. The difference being that the shell of the microspheres consists of a copolymer and that the encapsulated gas is a hydrocarbon. The key behind a foams highly reflective behavior is the thin wall of the bubbles which makes absorption unlikely to occur [19]. The difference in refractive index between the encapsulated gas, the sphere wall and the surrounding medium refracts the light. One foam bubble has little effect on the incoming light but the vast amount of bubbles present in foam clearly has an impact on the incoming light. The white color of foam is an example that illustrates this behavior. Dombrovsky suggested that the scattering of visible and infrared light by microspheres occurs at the contact zones between the microspheres [20]. Although he studied ceramic microspheres, the principles are the same.

2.3 Paint

The three major components in paint are solvent, binder and pigment. In addition to these, different additives such as anti foaming agents, fillers, UV stabilizers, thickeners, biocides, fungicides etc. are used to improve different properties. Pigments are used to give the paint a certain color and to improve hiding power. The main pigment used in this study is TiO_2 which is a white pigment. Other commonly used pigments are Fe_2O_3 and Cr_2O_3 . The perceived color is determined by the light source and absorption and reflection in the visual part of the spectrum. A blue pigment would for example have a reflectance peak around 450 – 490 nm and absorb in the other parts of the visual spectrum. The binder is essential in the film forming process when the paint dries or cures. It also has a large impact on adhesion and gloss. The film can be formed through physical or chemical processes depending on which type of binder that is used. Chemical processes include polymerization reactions which occur when the paint is applied to the substrate while physical processes can include evaporation of the solvent. The solvents used in paints are either water-based or oil-based. The purpose of the solvent is to dissolve the other components of the paint and to adjust the rheology of the paint. The paint used in this study is Tinova V from Nordsjö paint. By using a pre-mixed paint, the difficulties of combining solvent, binder and additives are avoided. Pigment volume concentration (PVC) and critical pigment volume concentration (CPVC) are two central concepts and comprises both pigment and filler. PVC and especially CPVC are linked to the binder's ability to wet the added pigment and filler. The CPVC is the maximum concentration of filler and pigment that allows the binder to completely wet the paint and thereby linked to the specific area of the added particles. Exceeding the CPVC often causes cracking of the paint as it dries [21].

There are a few traps to avoid when mixing microspheres into paint, especially when substituting the CaCO_3 filler with microspheres. The main thing to consider is the large difference in density. This difference is the reason for using vol% instead of wt%. When comparing paints in the way that is done in this paper, the trick is to keep the pigment concentration constant.

The brief explanation of the different components in paints given here is rather simplified. The real picture is much more complex but is outside the scope of this thesis project.

2.4 Spectrophotometry

A spectrophotometer generally consists of a light source, a monochromator, detector, and a display to report the results. It is used to measure optical properties such as reflectance or transmittance. Depending on which wavelengths that are measured, different light sources can be used. The actual instrument used in this study, PerkinElmer Lambda 900, uses a tungsten-halogen lamp for the VIS/NIR part of the spectrum and a deuterium lamp for the UV part. The sample is placed between the monochromator and the detector. The monochromator uses gratings to disperse the incoming light to different wavelengths or groups of wavelengths, depending on the resolution. There are a number of different kinds of detectors available on the market. The PerkinElmer Lambda 900 uses a photomultiplier tube for the UV-VIS part of the spectrum and a lead-sulfide detector for the NIR part. This specific spectrophotometer is also equipped with a 100 mm integrating sphere coated with Spectralon. Integrating spheres enables the measurement of diffuse reflectance. The difference between diffuse and specular reflection is illustrated in fig. 5.

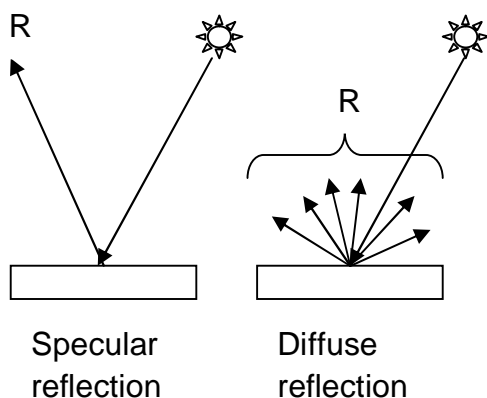


Figure 5. Illustrating the difference between specular and diffuse reflection.

2.5 Fourier Transform Infrared Spectroscopy (FTIR)

A FTIR instrument also measures optical properties but in the IR region of the spectrum. The instrument largely consists of a light source, an interferometer and a detector. In turn, the interferometer consists of a beamsplitter and two mirrors, one stationary and one moveable. When the radiation from the light source hits the beamsplitter, the beam is split into two beams by reflecting one part of the incoming light and transmitting the other part. The reflected light travels to the fixed position mirror where it is reflected and travels back to the beamsplitter. This light is once again split into two where the reflected part of the light is sent back to the source and the other part is transmitted

towards the detector. The transmitted rays (directly from the source) travel towards the moveable mirror and is reflected back in the same manner as in the case with the stationary mirror. One part is transmitted and travels back to the source and the other part is reflected towards the detector. This means that the separated beams are recombined when traveling to the detector, minus the parts which travel back to the source. The displacement of the moveable mirror is half the distance the light has travelled which is equal to δ , called the retardation. Depending on the distance between the moveable mirror and the beamsplitter compared to the distance between the stationary mirror and the beamsplitter, the recombined rays traveling towards the detector behave differently. If the moveable mirror is not displaced compared to the stationary mirror, the distances are equal and this is shown in the interferogram (the output of the interferometer) as a maxima. This is also the case if $\delta = n\lambda$, where n is an integer. A minima occurs in the case of destructive interference, which is the case if δ is an $n/2$ multiple of the wavelength λ . The interferogram can be expressed as an integral:

$$I(\delta) = \int_0^{\infty} B(\nu) \cos(2\pi\delta\nu) d\nu \quad (8)$$

Where $B(\nu)$ is the intensity of the source and ν is the wavenumber. To be able to convert the interferogram to an infrared spectrum, Fourier transformation is used. The maximum theoretical resolution, $\Delta\nu$, of an FTIR instrument is determined by

$$\Delta\nu = \frac{1}{\delta_{\max}} \quad (9)$$

The main advantage of FTIR compared to traditional dispersive instruments, is the signal-to-noise ratio. The reason behind this advantage is that the FTIR uses a continuum light source instead of measuring one wavelength, or wavenumber, at a time. Dispersive instruments would be much more time consuming if the same signal-to-noise ratio was to be achieved [22].

Given that the sample is opaque, measuring the reflectance enables calculation of the emissivity by using eq. 2 and 3.

3 Experimental

3.1 Paint formulations

The expansion of 20 μm (the size refers to the diameter) microspheres was conducted using a hot air oven with controlled temperature and constant stirring. The expanded microsphere densities were determined using a pycnometer. In order to avoid agglomeration, SiO_2 (Sipernat) was added to one batch (called DET) of microspheres before the expansion. Tioxide TR 88 was used as a white pigment. The other microspheres used in this study (10, 18, 40 and 80 μm) were already expanded.

The paint formulations consisted of binder (Tinova V, Nordsjö), TiO_2 dispersion and additives such as CaCO_3 , glass spheres, Expancel® microspheres etc. The TiO_2 dispersion was prepared by mixing 240 g Tioxide TR 88, 8.5 g orotan (acting as a dispersing agent) and 50 g of H_2O in a Silverson SL2T mixer for 5 minutes. To further remove agglomerates the paint formulations were mixed using a dissolver disk operated at 1800 rpm during 5 minutes. The paint samples were then placed in a vacuum chamber to remove air from the paints. Draw downs of the paints were made (three per sample) on Leneta opacity charts. The wet thickness of the draw downs were 1500, 1000 and 500 μm . The thickness of the dried draw downs were 600, 400 and 200 μm respectively. Draw downs with wet thickness of 250 μm was also made with eight of the samples (reference, coexpanded, 30% MS, 30% DET and the four blue samples). The dry thickness of these draw downs were 150 μm .

The paint formulations labeled “coexpanded” were produced by mixing microspheres, TiO_2 and SiO_2 prior to the expansion. This was done by mixing the dry powders in a plastic beaker containing small glass beads. The glass beads were removed with an 800 μm sieve. The coexpansions were aiming at microsphere particle size of around 10 μm . SEM images were taken with a Philips XL 20. The particle size of the coexpanded spheres was determined by laser diffraction using a Malvern Mastersizer 2000. The microsphere density was determined by measuring the total density of the mixture with a pycnometer (average of four measurements) and subtracting the contribution from TiO_2 and SiO_2 . Four of the paint formulations (Reference, Insuladd, Glass S38 and DET) were also color matched at a local paint shop, labeled with the prefix “Blue”. A number of competing systems including Insuladd, different glass spheres and the ceramic microsphere called Zeeosphere were also evaluated. A compilation of the samples is presented in table 1.

Table 1. Composition of the paint systems expressed in vol%.

	Tinova V [vol%]	TiO ₂ dispersion [vol%]	Additives				Particle size additive [μm]
			CaCO ₃ [vol%]	MS [vol%]	Glass spheres [vol%]	Insuladd [vol%]	
Reference	66	4	30	0	0	0	6
10% MS	66	4	20	10	0	0	20
20% MS	66	4	10	20	0	0	20
30% MS***	66	4	0	30	0	0	20
30% MS DET	66	4	0	30	0	0	20
30% MS 10 μm	66	4	0	30	0	0	10
Glass (K1)	66	4	0	0	30	0	100
Insuladd	66	4	0	0	0	30	100
Coexpanded	66	4	0	30	0	0	20
Blue Reference	70*	0	30*	0	0	0	6
Blue Insuladd	70*	0	0	0	0	30	100
Blue 30% MS	70*	0	0	30*	0	0	20
Blue Glass (S38)	70*	0	0	0	30	0	40
Glass(S38)/MS 30/0	66	4	0	0	30	0	40
Glass(S38)/MS 20/10	66	4	0	10	20	0	40/20
Glass(S38)/MS 10/20	66	4	0	20	10	0	40/20
Glass(S38)/MS 0/30***	66	4	0	30	0	0	20
10wt% TiO ₂ 30% MS	64	6	0	30	0	0	20
10wt% TiO ₂ Ref	64	6	30	0	0	0	5,5**
15wt% TiO ₂ 30% MS	61	9	0	30	0	0	20
15wt% TiO ₂ Ref	61	9	30	0	0	0	5,5**
30% MS d70	66	4	0	30	0	0	20
Zeeosphere	66	4	0	0	0	0	4
Binder + TiO ₂	96	4	0	0	0	0	-
461DET40	66	4	0	30	0	0	40
461DET80	66	4	0	30	0	0	80

* The Blue samples volume percentages represent the composition of the paint before they were color matched. ** The reference samples for 10 and 15wt% TiO₂ contained a different brand of CaCO₃, namely Omya BLP2 with a d(0.5) of 5.5 μm. ***The samples 30%MS and Glass(S38)/MS 0/30 are identical, they share the same ingredients but were prepared separately.

3.2 Dirt Pick-Up

The dirt pick-up studies were performed at SP Technical Research Institute of Sweden in Stockholm. Draw downs were made on thin steel plates using four different paint formulations (Reference, 30% MS DET, 30% MS and Coexpanded) with a dry thickness of around 400 μm . Duplicates of every sample were made. The dirt was prepared by mixing 8.5 g of carbon black (Degussa, FW200), 35 g of minerals (APPIE, JIS test powder 1 class 8) and 6.5 g of pitch (Koppers, special pitch no. 5). One gram of dirt was mixed with 1 g of butyl glycol and 998 g of distilled water. $L^*a^*b^*$ values were measured using an X-Rite SP62-162 portable spectrophotometer. $L^*a^*b^*$ measurements were conducted before the samples were sprayed with dirt the first time. The samples were sprayed with the dirt mixture and then dried in an oven at 50 °C for 30 min. The samples were placed at around a 30° angle when sprayed. This procedure was repeated two more times. After drying, the $L^*a^*b^*$ (CIELAB color space, see section 4.3) values were measured at the upper left, middle and lower right part of the plates.

3.3 Optical Measurements

The optical properties in the visual part of the spectrum (360 – 740 nm) were conducted using a Konica Minolta CM-3610d spectrophotometer. The UV-VIS-NIR (300 – 2500 nm, 5 nm resolution) reflectance measurements were conducted at Uppsala University using a Perkin Elmer Lambda 900 spectrophotometer (see section 2.4) equipped with an integrating sphere. IR reflectance was measured by using a Bruker Tensor 27 FTIR instrument with an integrating sphere. FTIR measurements were conducted at Uppsala University using 300 scans between 450 and 4000 cm^{-1} with a resolution of 4 cm^{-1} . FTIR measurements were only conducted on the 600 μm samples.

Solar reflectance index calculations were performed using an excel spreadsheet coded by Levinson from Lawrence Berkeley National Laboratory Heat Island Group [23].

3.4 Contact Angle

Measurements were performed by SP Technical Research center in Stockholm. Five different samples were studied, the reference sample containing 30vol% CaCO_3 and the four Glass/MS samples. Draw downs of the four glass/MS samples and the reference sample were made with a dry thickness of 400 μm on standard glass substrates.

4 Results and Discussion

4.1 Optical Measurements

The emittance values were calculated using eq. 5 and 6 as previously described. The results for all samples were within the range 0.90 – 0.93 and are therefore presented appendix A. A selection of R_{sol} values are presented in this section. The calculated R_{sol} values for all the samples, including different thicknesses, are also presented in appendix A.

First of all, it is important to remember that the reflectance data presented in this paper are meant for relative comparisons. The paint systems used are far from optimized. A commercial paint contains a large number of additives as mentioned in section 2.3. These paints are based on the paint Tinova V, which is considered to be a more or less pure binder system. This is not entirely true since it also contains 6% talc along with different modifiers.

The spectrum in fig. 6 depicts the reflectance spectrum from 300 to 2500 nm. The results from the pre-study using a VIS spectrophotometer are consistent with the results from the UV-VIS-NIR spectrophotometer. The samples included in fig. 6 all contain TiO_2 , while the color matched blue samples in fig 7. do not. Instead they absorb in most of the visual part of the spectrum apart from the peak at around 450 nm which is responsible for their blue appearance. Unfortunately, the pigments used to color match the blue samples are unknown. There are however some similarities between fig. 6 and 7. The samples with the highest reflectance values both contain thermoplastic microspheres.

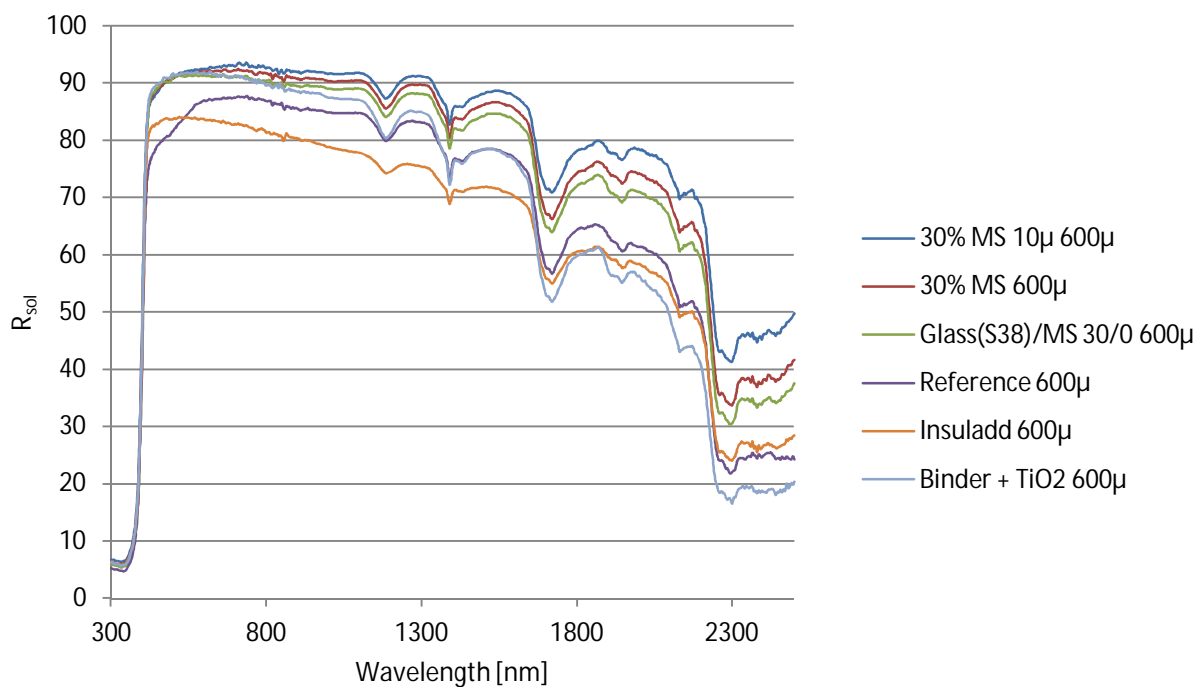


Figure 6. Reflectance spectrum ranging from 300 – 2500 nm for a selection of 600 μ m samples. All samples contains the same amount of TiO₂.

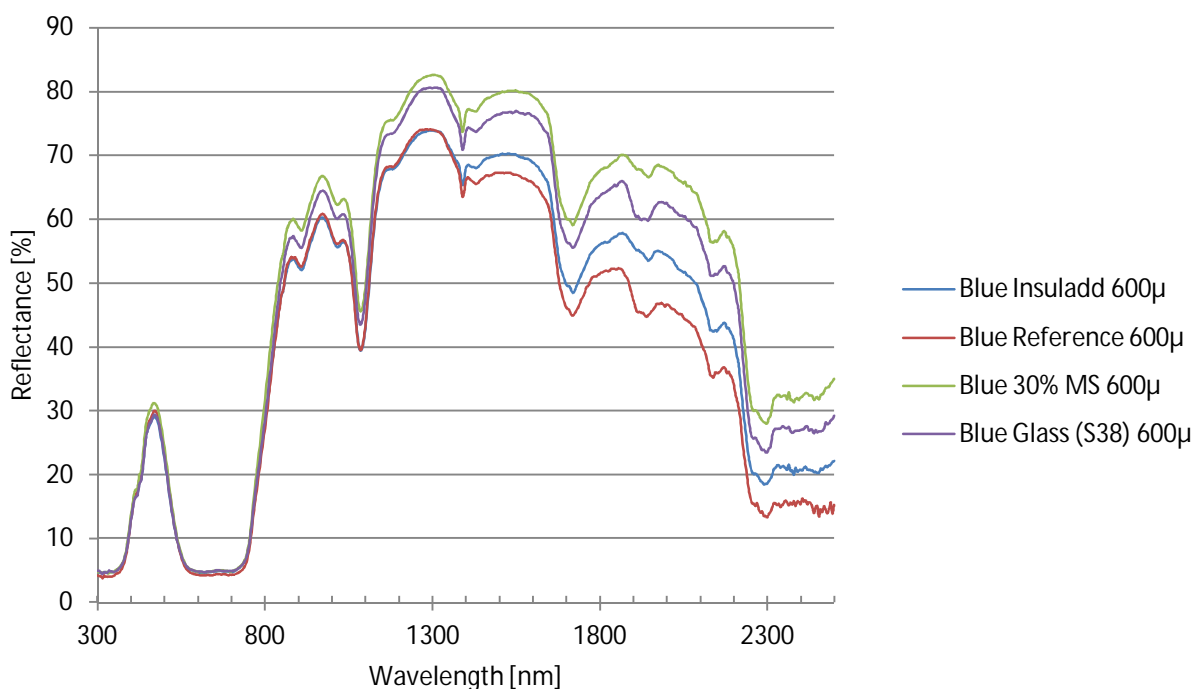


Figure 7. Reflectance spectrum of color matched blue paints. Measurements were done between 300 and 2500 nm.

Figure 8 presents the calculated R_{sol} values for the blue samples. The relatively low solar reflectance values are due to blue pigments low reflectance values in the visible part of the spectrum. The sun peaks in the visual part of the spectrum which is taken into consideration when calculating R_{sol} . These paints all absorb a great deal of the incoming light at those wavelengths which only leaves the NIR part of the spectrum. If the VIS part were ignored when calculating R_{sol} , the difference between the samples in fig. 8 would have been larger.

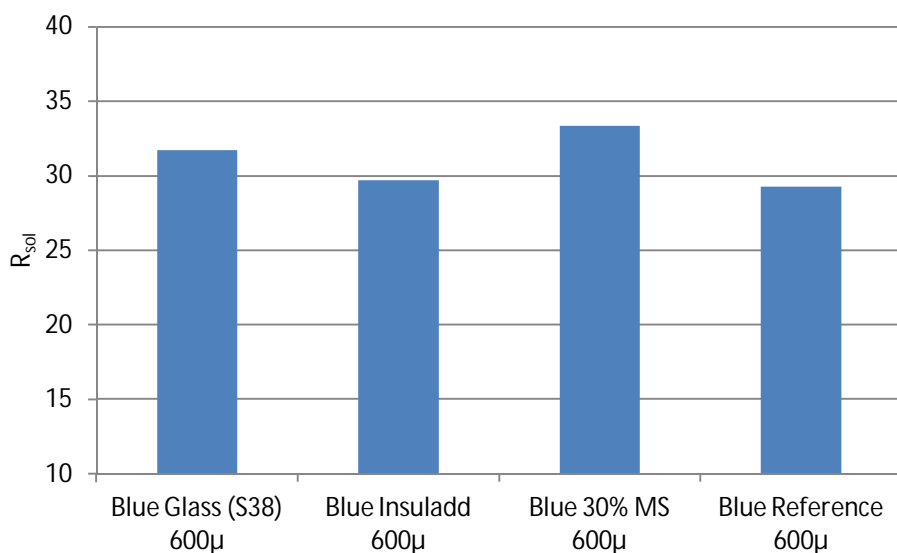


Figure 8. Comparison of R_{sol} between the color matched blue paints.

The glass/MS samples in fig. 9 show a slight increase in reflectance values for increasing amounts of thermoplastic microspheres. One must remember that the different spheres (glass 40μm and thermoplastic microspheres 20μm) differ in size. It is not a straight off comparison between glass and thermoplastic microspheres which can be seen in fig. 10 where 40 μm spheres are compared. The data presented in fig. 10 indicate no difference in R_{sol} values between the glass and thermoplastic microspheres. The difference in R_{sol} between these two samples are only 0.3 (84.1 and 83.8, based on a single measurement). These results also indicate that the increase in reflectance for thermoplastic microspheres compared to glass microspheres in fig. 9 is an effect which can be attributed to particle size. It can be seen that paints containing smaller spheres have higher reflectance values than the ones containing larger spheres. One example of this is the comparison between 10μm and 20 μm thermoplastic spheres. This study relies on comparing different additives while keeping the TiO_2 concentration constant. The additive concentration is in many cases kept at 30 vol%. By using smaller microspheres, a larger number of microspheres are present in the paint which can interact with the incoming light.

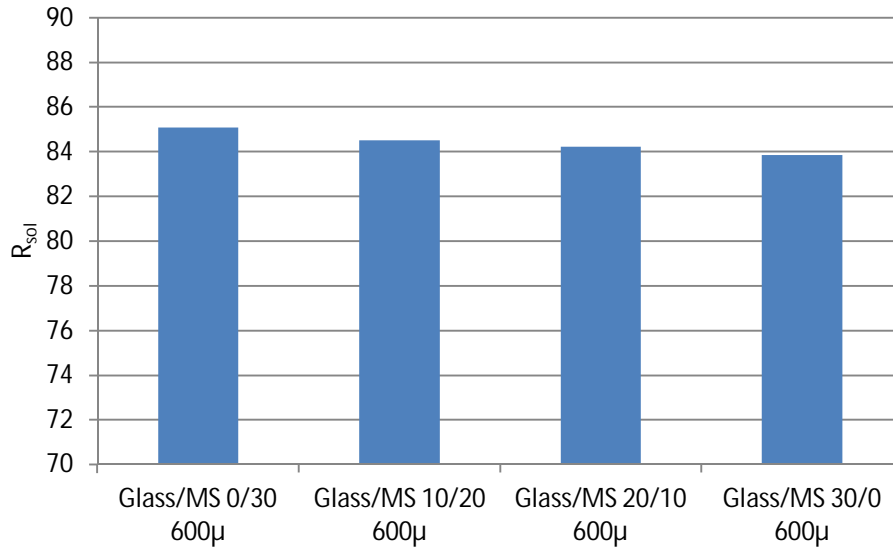


Figure 9. R_{sol} values for different compositions of glass/MS samples. 0/30 stands for 0vol% glass spheres and 30vol% thermoplastic microspheres.

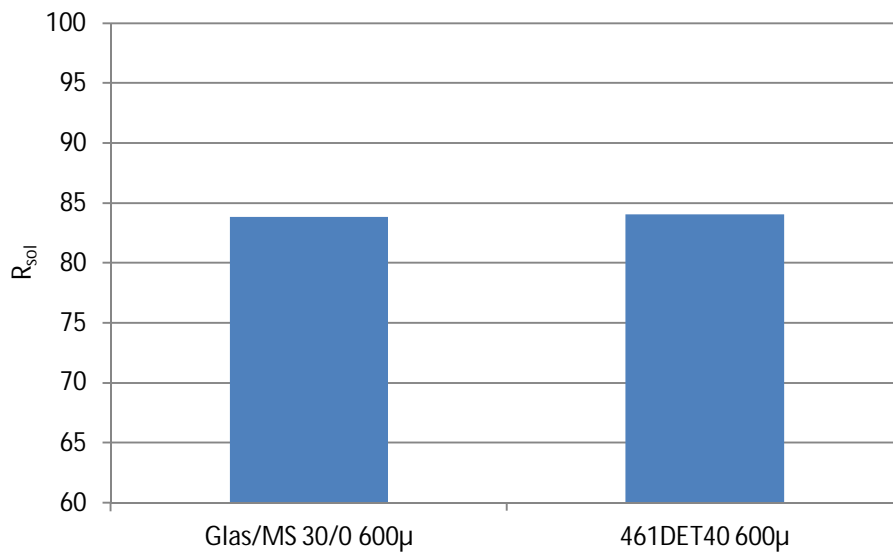


Figure 10. Comparison of glass and thermoplastic microspheres, both spheres are 40 μm in diameter.

A similar comparison is presented in fig. 11, but with CaCO_3 instead of glass spheres. The data clearly show that replacing CaCO_3 with microspheres has a positive effect on R_{sol} . For every 10% increment, there is roughly an increase of two units of R_{sol} . It should be mentioned that CaCO_3 with different particle sizes behave slightly different in regard to reflectivity.

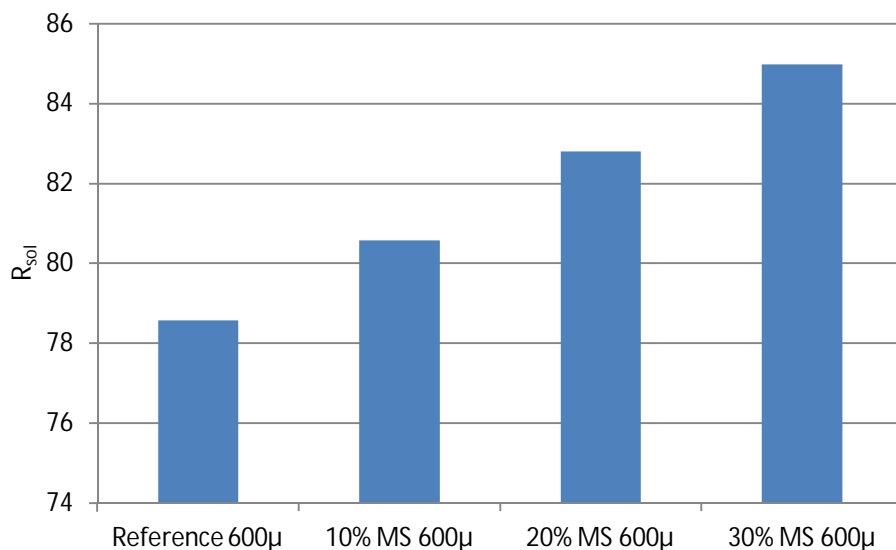


Figure 11. Substituting CaCO_3 for thermoplastic microspheres increases R_{sol} . The microspheres used are 20 μm in diameter.

The impact that the microsphere particle size has on R_{sol} is illustrated in fig. 12. These data are consistent with the result of the previous unpublished study performed by Expancel®. By decreasing the particle size of the spheres, R_{sol} is increased. This is also the case for glass spheres but the difference lies once again in the density. A glass sphere with a diameter of 10 μm would have a much higher density and therefore add a significant amount of weight to the paint system. As previously mentioned a fix volume of additive (microspheres) was added to each paint and using small microspheres instead of larger ones results in a larger number of microspheres in the paint. The results in fig. 12 are consistent with this theory along with the foam theory described in section 2.2.

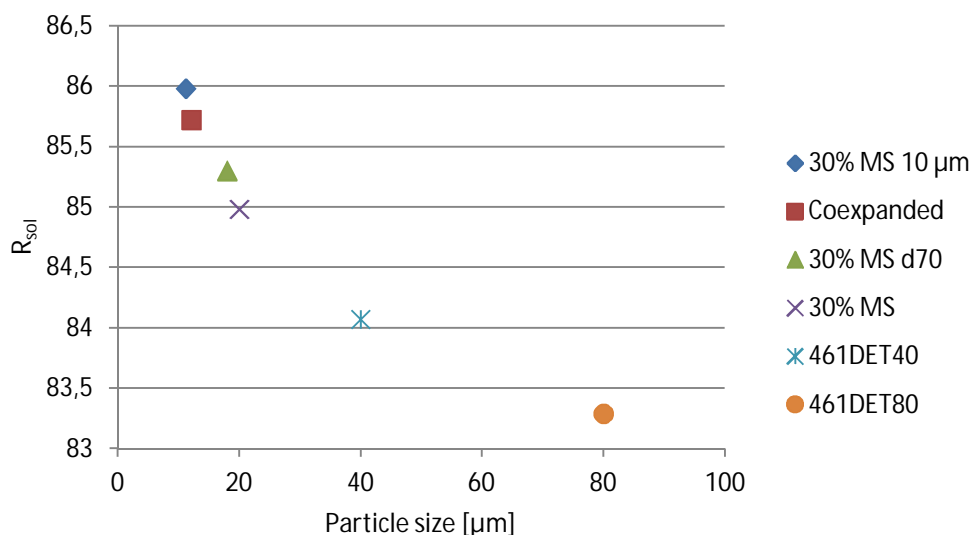


Figure 12. Particle size dependency of R_{sol} . Paints containing smaller microspheres have higher reflectance values and vice versa. All the samples included in this figure were 600 μm thick.

The thickness of the paint layer and its impact on R_{sol} is illustrated in fig. 13 for two different types of paint, 30% MS and the CaCO_3 containing reference, both containing TiO_2 . Thicker samples show higher R_{sol} values. The thinner samples are less opaque which means that the substrate has an impact on the reflectance. Since the substrate is the black part of a Leneta opacity chart, it provides no further increase in reflectivity (at least in the visual part of the spectrum). One can clearly see that the lower R_{sol} values for thinner samples are consistent for all measured samples (see appendix A).

The positive effect of adding microspheres to paint is believed to diminish as the TiO_2 content is increased. Therefore, samples with 10 and 15 wt% TiO_2 were also prepared. The results from R_{sol} calculations on these samples with associated references are presented in fig. 14. There is a slight decrease in the difference between the reference sample and the one containing microspheres for the 15 wt% sample compared to the 10 wt% sample (5.6 compared to 6.2). The decrease is considered to be too small to be able to back up the previous statement. One reason for this could be that the TiO_2 content in the measured samples are too low to be able to detect this effect.

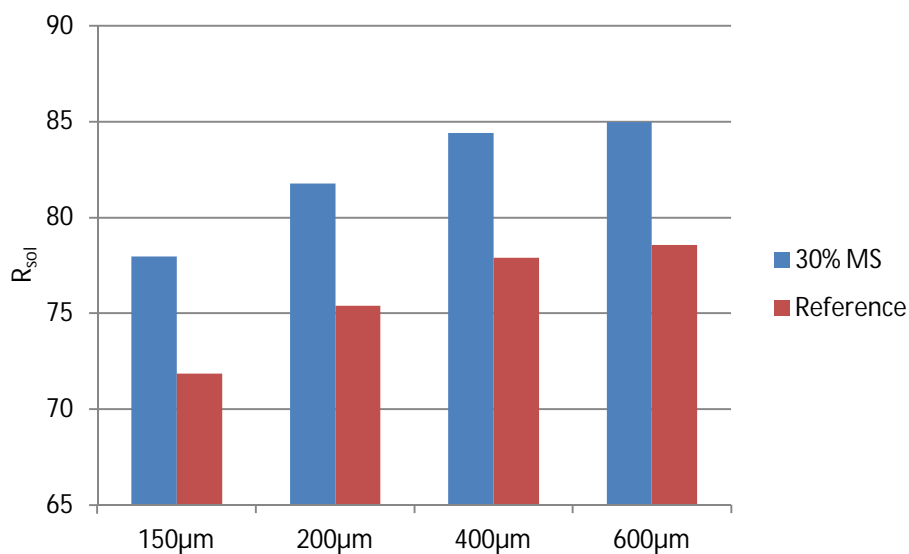


Figure 13. R_{sol} variations for different thicknesses of the 30% MS and Reference samples.

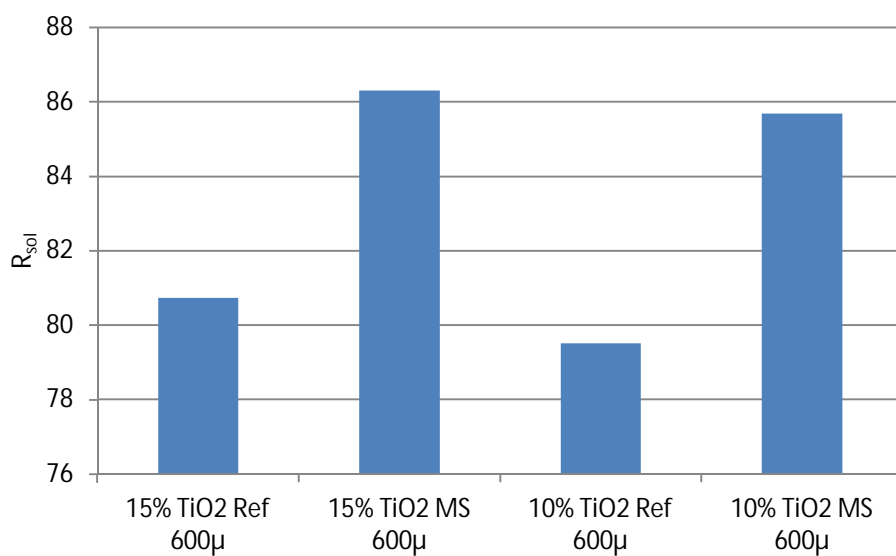


Figure 14. R_{sol} values for reference and MS samples with increased amount of TiO₂.

The solar reflectance index presented in fig. 15 is a measure of how “cool” the paints are. Since the emittance data do not differ more than 0.3 (0.90 – 0.93) percentage points between the samples, the emittance has little or no impact on the SRI. The blue samples low SRI scores are explained by their low reflectivity in the visual part of the spectrum.

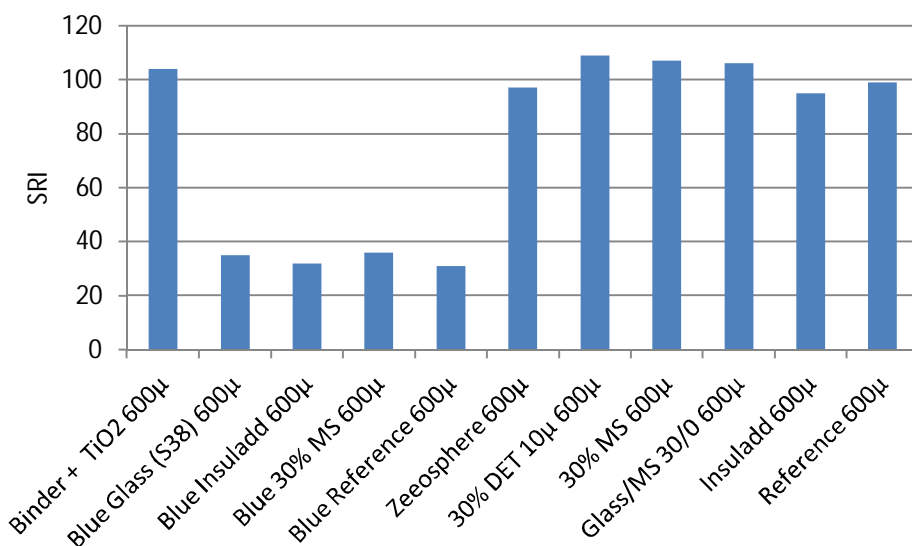


Figure 15. Solar Reflectance Index for a number of samples. Full data set is presented in appendix A.

4.2 Coexpanded Spheres

When adding pigment to paint, it is important to avoid agglomeration of the pigment in order to use it effectively. TiO₂ is often a relatively expensive part of the paint. The supposed benefit of coexpanded microspheres compared to uncoated microspheres is the more effective use of the added TiO₂. By coating the microspheres with pigment, the pigment particles are spread out on the surface of the microspheres. The idea is that this process should prevent agglomeration of the pigment. In an ideal case, only primary particles of TiO₂ would be present in the paint. The grinding and sieving of the TiO₂ was done in an attempt to reduce the amount of TiO₂ agglomerates. However, despite these attempts the SEM pictures (fig. 16) of the coexpanded spheres show that these types of agglomerates are present. It should be noted that the SEM images and particle size measurements were done on a different batch (with similar total density, 313 g/dm³) than the one used to make the paint (267 g/dm³). This was a necessity due to the fact that particle size measurement consumes a certain amount of sample that cannot be collected afterwards. The coexpansion was set up as a batch process in order to avoid the problem with inhomogeneous samples. Another challenge in making coexpanded spheres is the microsphere density. The density is linked to the particle size via the expansion process. In order to conduct a fair comparison between coated and uncoated spheres, similar densities and particle sizes should be used. The results from the particle size measurements, presented in fig. 17 ($d(0.5) = 12.1\mu\text{m}$), is a bit higher than expected. The detection of large particles (up to 100 µm) is explained by agglomeration of the microspheres which can be seen in the right hand SEM image in fig. 16. The

density was calculated to be around 65 g/dm^3 based on the total density of 267 g/dm^3 . Comparison of these data with the ones from the $10 \text{ }\mu\text{m}$ samples ($11.2 \text{ }\mu\text{m}$ and 141 g/dm^3), raises the suspicion that the coexpanded data are not representative. This could be explained by the fact that the particle size 12.1 originates from the batch with the total density 313 g/dm^3 . The batch used (267 g/dm^3) should in fact contain microspheres larger than $12.1 \text{ }\mu\text{m}$. Fig. 12 compares samples of different particle sizes with the coexpanded spheres. The sample closest to $12.1 \text{ }\mu\text{m}$ is the 30% MS $10 \text{ }\mu\text{m}$ ($11 \text{ }\mu\text{m}$). The R_{sol} values show no indication of any positive effect of coexpanding the spheres with TiO_2 compared to the “ordinary” samples. But bear in mind that the particle sizes/densities differ. The coexpansion process is far from optimized and many questions are yet to be answered.

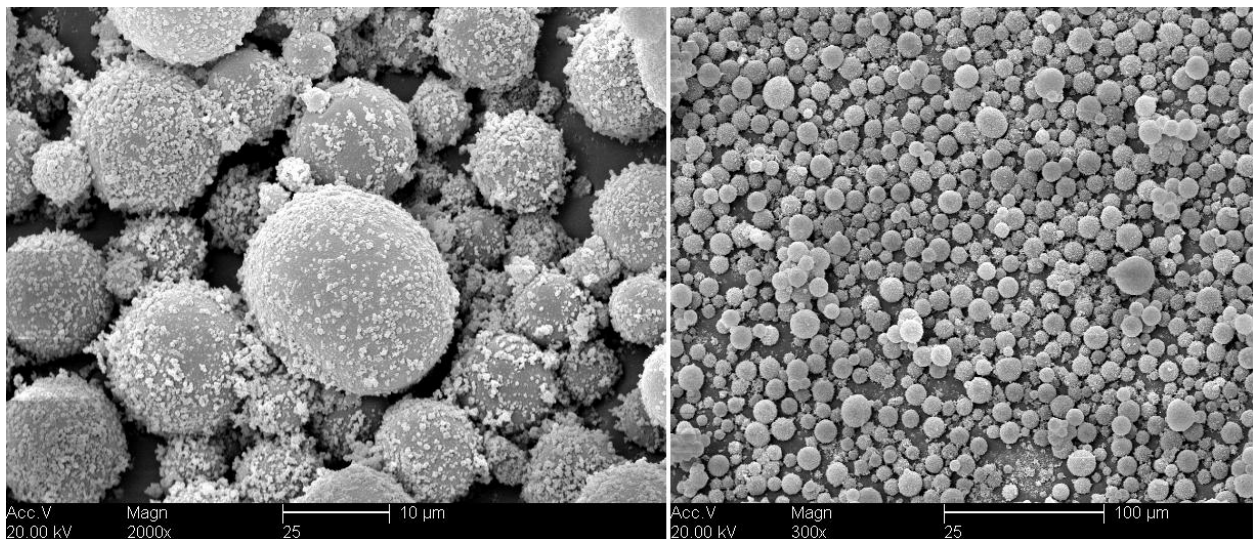


Figure 16. SEM images of coexpanded spheres.

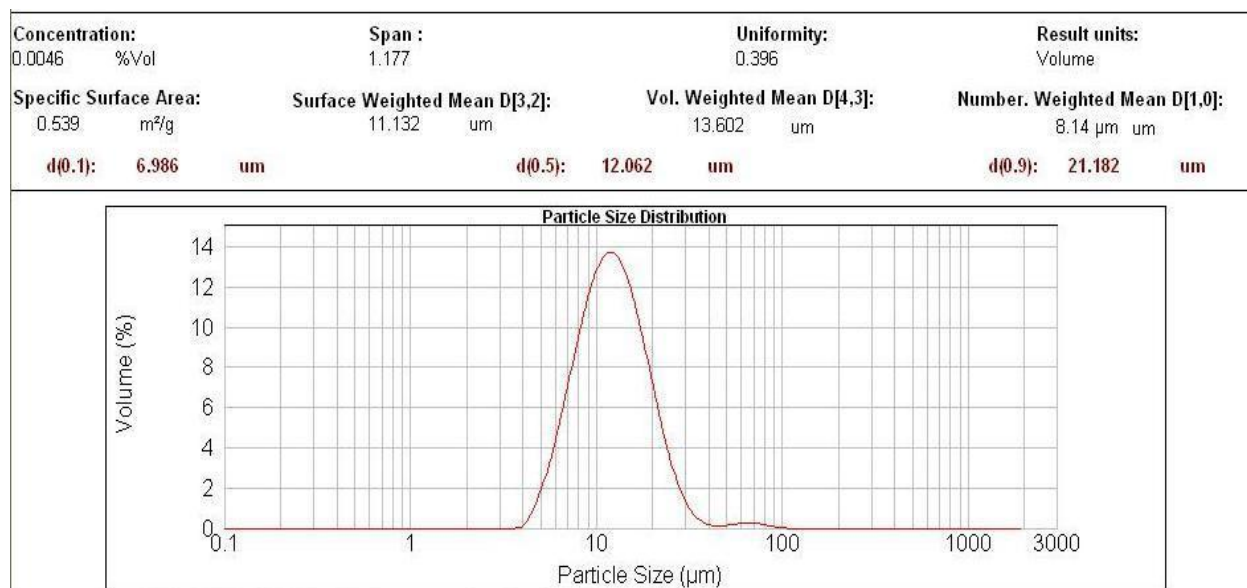


Figure 17. Particle size distribution curve for coexpanded spheres. The fraction on the right side of the peak can be an indication of microsphere agglomerates or simply large microspheres.

4.3 Dirt Pick-Up

The dirt pick-up study conducted at SP suffers from relatively large errors. For the CIELAB evaluation, the L^* values were measured using a hand held device. The CIELAB color space uses the L^* , a^* and b^* as coordinates. L^* being the lightness parameter and a^* and b^* defining the different colors [16]. Since each sample was not evenly covered with dirt, this could give rise to a relatively large error source. A second error arises due to the fact that the samples were placed at a somewhat arbitrary angle when sprayed with the dirt mixture. An accumulation of dirt was seen at the lower end of the samples. Three measurements per sample were made. The measurements from the upper left and middle part of the samples are more likely to suffer from these kinds of errors. In these areas, small spots were significantly darker than their surroundings. The measurements done in the lower right corner of the samples were more evenly covered with dirt because of the angle the samples were positioned at as previously mentioned. The data are presented in fig. 18 and suggest no significant differences in resistance to dirt pick-up.

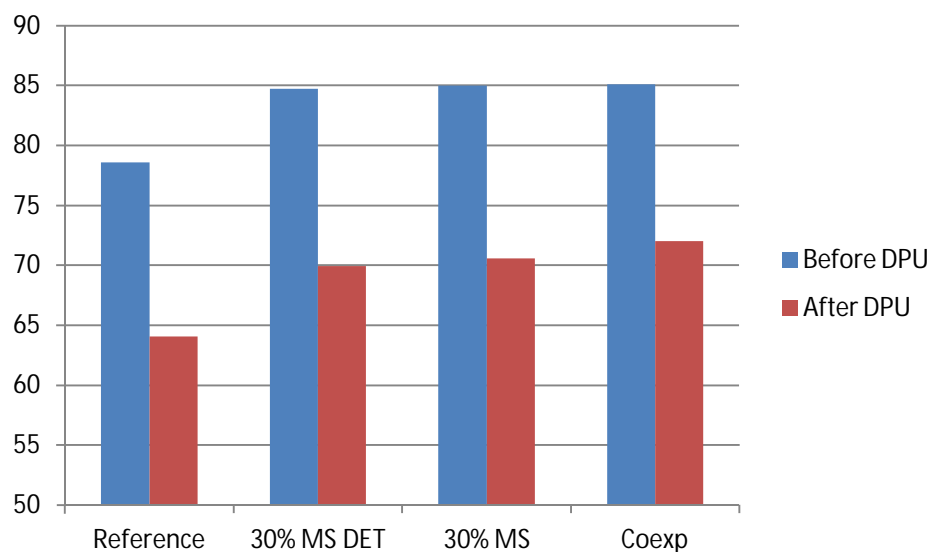


Figure 18. Comparison of R_{sol} values before and after Dirt Pick-Up.

4.4 Contact Angle

Figure 19 presents a bar graph showing the average values from the contact angle measurements. Error bars indicate the standard deviation of each sample. A table containing all data from these measurements is found in the appendix B. The first data point for Glass(S38)/MS 10/20 is considered to be an outlier and is not included in figure 19. Raw data is presented in appendix B.

The contact angle measurement data show that the reference sample was the most hydrophilic and that the samples containing thermoplastic microspheres were the most hydrophobic. A hydrophilic surface subjected to water can create a thin water film which could aid the transportation of dirt from the surface, thus cleaning it. The sample 30% MS used in the dirt pick-up study and the sample Glass(S38)/MS 0/30 used in the contact angle measurements are identical but prepared separately. The reference samples used in the two measurements is the same TiO_2 containing reference. The supposed effect of the hydrophilicity of the reference sample was not detected since the dirt pick-up samples were never exposed to water. Therefore no correlation between the dirt pick-up study and the contact angle measurements were found.

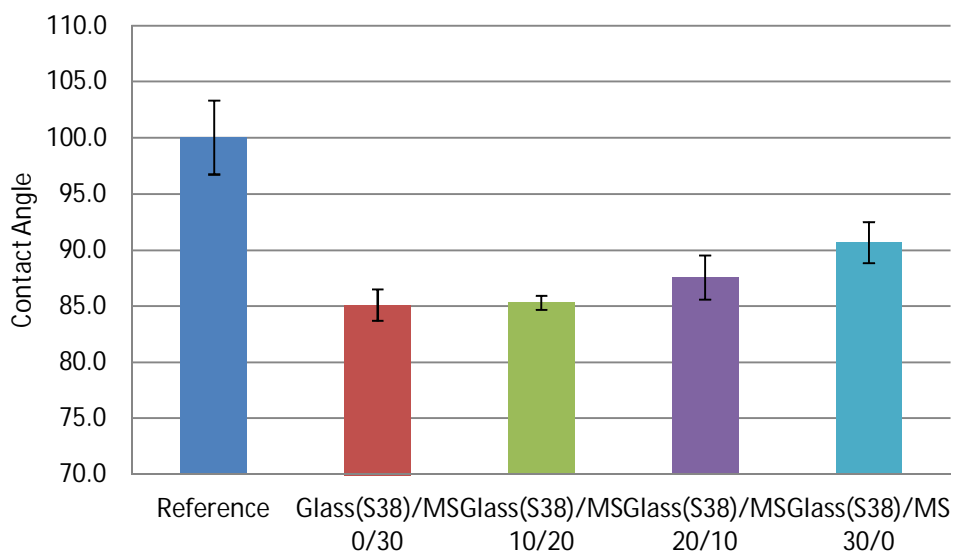


Figure 19. Results from contact angle measurement. Error bars indicate the standard deviation of each sample.

4.5 Filler (CaCO_3)

Two different types of CaCO_3 particle sizes were initially tested as reference samples, Socal P2 with a particle size between 0.18 – 0.55 μm and Durcal 5 with a particle size of 6 μm . All three draw downs (1500, 1000 and 500 μm wet thickness) made with the paint containing Socal P2 showed significant cracking. Only the 1500 μm draw down made with the Durcal 5 paint showed signs of cracking. For that reason Durcal 5 was used from there on. Small particles have larger surface area than larger particles and push the PVC towards and sometimes beyond the CPVC. The reason why the thicker draw downs were more prone to cracking is the evaporation of the solvent and the contraction of the paint as it dries. By using an additive with lower surface area one can achieve higher PVC without causing the paint to crack and thus using less binder. One thing to keep in mind is that the smaller spheres showed higher R_{sol} values which force a compromise when deciding on which type of additives to use.

5 Conclusions and Future Work

It can be concluded that the addition of microspheres to the types of paints examined in this study enhance the reflectance. It is also evident that the particle size of the additive plays a major role where smaller spheres perform better than larger spheres. The same behavior is seen for glass spheres.

The coexpanded spheres did not behave as predicted. No difference in reflectivity between coexpanded and “ordinary” microspheres was found. The particle size of the coexpanded spheres did not match the “ordinary” spheres which causes the comparison to favor the latter. Future work is needed in order to fully evaluate the coexpanded spheres. Examples of this work would be to match particle sizes, examine the effect of different polymer shells, reduce agglomerates of TiO_2 and examine how much TiO_2 is needed for an optimal coating of the microspheres.

The dirt pick-up study showed no difference in dirt resistance between the reference sample and samples containing microspheres. Future work in this area could examine how the different samples are affected by weathering tests.

In order to draw any real conclusions concerning dirt resistance from the effect of the hydrophobic character of the thermoplastic microspheres, dirt pick-up studies and contact angle measurements should be done in combination with weathering tests.

The blue paint containing microspheres (Blue 30% MS) showed greater R_{sol} values than the blue reference paint. Future work is needed to examine if this is the case for other colors/pigments. A more extensive study concerning the addition of microspheres to non-white paints is needed to be able to draw any conclusions about the effect of thermoplastic microspheres in other paints. The results presented in fig. 7 and 8 indicate positive effects for the addition of microspheres in combination with this specific pigment and it is considered likely that this would be the case for other system as well.

Acknowledgments

I would like to thank Annica Nilsson for taking the time to be my supervisor at Uppsala University and especially for letting me use the spectrophotometer and FTIR instrument at Solid State Physics. I would like to give special thanks to my supervisor at Expancel® Jan Nordin and Jonas Vestin for all the help during this semester. Last but not least, I would like to thank Tomas Gardfors for always taking the time to discuss different aspects of this project and the RD&I department for giving me the opportunity to conduct my master thesis at Expancel®.

References

- [1] P.A. Mirzaei, F. Haghighat, "Approaches to study Urban Heat Islands – Abilities and limitations", *Building and Environment*, 45, 2192 – 2201, 2010
- [2] T.R. Oke, G.T. Johnson, D.G. Steyn, I.D. Watson, "Simulations of Urban heat island under 'ideal' conditions at night Part 2: Diagnosis of causation", *Boundary-Layer Meteorology*, 56, 339 – 358, 1991
- [3] A. Synnefa, M. Santamouris, K. Apostolakis, "On the development, optical properties and thermal performance of cool colored coatings for the urban environment", *Solar Energy*, 81, 488 – 497, 2007
- [4] H. Akbari, M. Pomerantz, H. Taha, "Cool surfaces and shade trees to reduce energy use and improve air quality in urban areas", *Solar Energy*, 70, 295 – 310, 2001
- [5] Energy Information Administration (EIA), *Annual Energy Review*, 2007
- [6] H. Taha, "Modeling the impact of large-scale albedo changes on ozone air quality in the south coast air basin", *Atmospheric Environment*, 31, 1667 – 1676, 1997
- [7] H. Taha, "Urban surface modification as a potential ozone air-quality improvement strategy in California: A mesoscale modeling study", *Boundary-Layer Meteorology*, 127, 219 – 239, 2008
- [8] <http://www.energy.ca.gov/title24/coolroofs> (2013-05-21)
- [9] <http://www.energycodes.gov/resource-center/policy/green-roof-improvement-fund-chicago-il-2006> (2013-05-21)
- [10] <http://www.nyc.gov/html/coolroofs/html/about/about.shtml> Philadelphia title 4 (2013-05-21)
- [11] C.G. Granqvist, "Radiative heating and cooling with spectrally selective surfaces", *Applied Optics*, 20, 2606-2615, 1981
- [12] J.R. Simpson, E.G McPherson, "The effect of roof albedo modification on cooling loads of scale model residences in Tucson, Arizona", *Energy and Buildings*, 25, 127 – 137, 1997
- [13] R. Levinson, H. Akbari, "Potential benefits of cool roofs on commercial buildings: conserving energy, saving money and reducing emission of greenhouse gases and air pollutants", *Energy Efficiency*, 3, 53 – 109, 2010
- [14] <http://heatisland.lbl.gov/sites/heatisland.lbl.gov/files/Cool-roof-Q+A.pdf> (2013-05-21)
- [15] M. Santamouris, A. Synnefa, T. Karlessi, "Using advanced cool materials in the urban built environment to mitigate heat island and improve thermal comfort conditions", *Solar Energy*, 85, 3085 – 3102, 2011
- [16] A. M. Nilsson, "Daylighting Systems", *Doctoral Thesis*, Uppsala, 2012
- [17] G.B. Smith, C.G. Granqvist, "Green Nanotechnology – Solutions for Sustainability and Energy in the Built Environment", *CRC Press*, 2011

- [18] P. Berdahl, S.E. Bretz, "Preliminary survey of the solar reflectance of cool roofing materials", *Energy and Buildings*, 25, 149-158, 1997
- [19] C.F. Bohren, "Clouds in a glass of beer", Dover Publications Inc., 2001
- [20] L. A. Dombrovsky, "Approximate models of radiation scattering in hollow-microsphere ceramics", *High Temperature*, 42, 776 – 784, 2004
- [21] P. Flodin, "Kompendium i polymerteknologi", Chalmers tekniska högskola
- [22] W.D. Perkins, "Fourier transform-infrared spectroscopy: Part 1. Instrumentation", *Journal of Chemical Education*, 63, A5 – A10, 1986
- [23] <http://heatisland.lbl.gov/content/sri-calculator> (2013-05-21)

Appendix A

Table 2. R_{sol} , emittance and SRI data for all samples.

Sample name	R_{sol}	ϵ	SRI
Binder + TiO ₂ 200 μ	78.31	-	-
Binder + TiO ₂ 400 μ	81.60	-	-
Binder + TiO ₂ 600 μ	82.53	0.91	104
Blue Glass (S38) 150 μ	27.60	-	-
Blue Glass (S38) 200 μ	30.06	-	-
Blue Glass (S38) 400 μ	31.48	-	-
Blue Glass (S38) 600 μ	31.74	0.91	35
Blue Insuladd 150 μ	25.02	-	-
Blue Insuladd 200 μ	27.63	-	-
Blue Insuladd 400 μ	29.24	-	-
Blue Insuladd 600 μ	29.71	0.91	32
Blue 30% MS 150 μ	29.76	-	-
Blue 30% MS 200 μ	31.88	-	-
Blue 30% MS 400 μ	32.99	-	-
Blue 30% MS 600 μ	33.36	0.9	36
Blue Reference 150 μ	-	-	-
Blue Reference 200 μ	-	-	-
Blue Reference 400 μ	-	-	-
Blue Reference 600 μ	29.27	0.92	31
15% TiO ₂ Ref 200 μ	80.54	-	-
15% TiO ₂ Ref 400 μ	81.11	-	-
15% TiO ₂ Ref 600 μ	80.73	0.92	102
15% TiO ₂ MS 200 μ	84.63	-	-
15% TiO ₂ MS 400 μ	85.97	-	-
15% TiO ₂ MS 600 μ	86.30	0.91	109
Zeeosphere 200 μ	75.99	-	-
Zeeosphere 400 μ	77.81	-	-
Zeeosphere 600 μ	77.96	0.91	97
30% MS DET 150 μ	82.73	-	-
30% MS DET 200 μ	81.79	-	-

30% MS DET 400 μ	84.55	-	-
30% MS DET 600 μ	84.73	0.9	107
30% DET 10 μ 200 μ	84.26	-	-
30% DET 10 μ 400 μ	85.88	-	-
30% DET 10 μ 600 μ	85.98	0.91	109
30% MS 150 μ	77.96	-	-
30% MS 200 μ	81.76	0.91	103
30% MS 400 μ	84.39	0.91	106
30% MS 600 μ	84.98	0.91	107
461DET40 200 μ	81.25	-	-
461DET40 400 μ	83.58	-	-
461DET40 600 μ	84.07	0.91	106
461DET80 200 μ	79.02	-	-
461DET80 400 μ	82.76	-	-
461DET80 600 μ	83.29	0.91	104
30% MS d70 200 μ	83.40	-	-
30% MS d70 400 μ	85.06	-	-
30% MS d70 600 μ	85.30	0.91	107
10% TiO ₂ Ref 200 μ	77.60	-	-
10% TiO ₂ Ref 400 μ	79.95	-	-
10% TiO ₂ Ref 600 μ	79.51	0.92	100
10% TiO ₂ MS 200 μ	83.08	-	-
10% TiO ₂ MS 400 μ	85.50	-	-
10% TiO ₂ MS 600 μ	85.69	0.91	108
Coexpanded 150 μ	81.05	-	-
Coexpanded 200 μ	82.86	-	-
Coexpanded 400 μ	85.60	-	-
Coexpanded 600 μ	85.72	0.93	109
Glass K1 200 μ	77.42	-	-
Glass K1 400 μ	81.73	-	-
Glass K1 600 μ	82.89	0.92	105
Glass/MS 0/30 200 μ	82.35	-	-
Glass/MS 0/30 400 μ	84.69	-	-
Glass/MS 0/30 600 μ	85.08	0.91	107
Glass/MS 10/20 200 μ	81.26	-	-
Glass/MS 10/20 400 μ	84.17	-	-
Glass/MS 10/20 600 μ	84.51	0.91	107
Glass/MS 20/10 200 μ	80.35	-	-

Glass/MS 20/10 400μ	83.81	-	-
Glass/MS 20/10 600μ	84.23	0.91	106
Glass/MS 30/0 200μ	80.95	-	-
Glass/MS 30/0 400μ	83.36	-	-
Glass/MS 30/0 600μ	83.84	0.91	106
Insuladd 200μ	74.08	-	-
Insuladd 400μ	75.60	-	-
Insuladd 600μ	75.69	0.92	95
Ref DPU 1	64.22	-	-
Ref DPU2	63.93	-	-
DET DPU 1	69.04	-	-
DET DPU 2	70.80	-	-

DE DPU 1	69.79	-	-
DE DPU 2	71.34	-	-
Coexp DPU 1	72.59	-	-
Coexp DPU 2	71.41	-	-
Reference 150μ	71.85	-	-
Reference 200μ	75.41	-	-
Reference 400μ	77.89	-	-
Reference 600μ	78.57	0.92	99
10% MS Dur 200μ	77.31	-	-
10% MS Dur 400μ	79.99	-	-
10% MS Dur 600μ	80.58	0.91	102
20% MS Dur 200μ	79.34	-	-
20% MS Dur 400μ	82.24	-	-
20% MS Dur 600μ	82.80	0.9	104

Appendix B

Table 3. Data from contact angle measurements. Data point one from Glass(S38)/MS 10/20 is considered to be an outlier.

	Pt. 1	Pt. 2	Pt. 3	Pt. 4	Pt. 5	Average	Standard deviation
Ref II 30vol% CaCO ₃	103.1	98.2	103.8	94.8	100.4	100.1	3.30
Glass(S38)/MS 0/30	87.3	85.8	83.1	84.3	85.1	85.1	1.41
Glass(S38)/MS 10/20	67.0	86.1	85.0	85.7	84.5	85.3	0.62
Glass(S38)/MS 20/10	84.8	87.0	88.5	90.1	87.5	87.6	1.95
Glass(S38)/MS 30/0	88.9	92.5	88.2	92.7	91.1	90.7	1.84